STUDY OF FLUIDIC ROLL CONTROL
FOR SOUNDING ROCKET APPLICATIONS

by Carl G. Ringwall and William L. Keltz

August 1970

STUDY OF FLUIDIC ROLL CONTROL

FOR

SOUNDING ROCKET APPLICATIONS

By Carl G. Ringwall and William L. Keltz

August 1970

FOREWORD

This report summarizes the effort carried out
under Task II of Contract NAS 2-5467 with the
Ames Research Center, National Aeronautics
and Space Administration. The project engineer
at Ames Research Center is Mr. Dean M. Chisel.
The study was conducted by C. G. Ringwall,
R. K. Rose and W. L. Keltz.

TABLE OF CONTENTS

LIST OF ILLUSTRATIONS

1.0 SUMMARY AND CONCLUSIONS

This report describes results of a study to determine optimum fluidic implementation of roll control loops for a typical SPARCS* mission. This report section outlines the functions of the roll control loops, summarizes the fluidic implementation, and provides recommendations and conclusions. Detail descriptions of the control loops are provided in later sections of the report.

1.1 Background - The SPARCS Mission

During acquisition with SPARCS operation three distinct types of roll control are utilized; viz. during

1. despin
2. coarse acquisition
3. intermediate and fine acquisition.

During despin a roll-rate control despins an initially rolling payload (up to 3 rev/sec) to a rate near zero. The fluidic despin control can be augmented with a "yo-yo" mechanism, but always some or all of the despin impulse is provided by thrust from nozzles.

In the coarse control phase, large errors in pitch and yaw angle are quickly reduced to a maximum value of 10 degrees. During coarse control a roll control loop is employed to maintain roll rate of the vehicle to very near zero to decouple the pitch and yaw control loops.

Intermediate acquisition occurs when pitch and yaw errors are reduced below 10 degrees. During intermediate acquisition (and fine acquisition) a roll position loop is used to provide the desired final attitude of the payload.

Intermediate and fine acquisition differ only in the maximum thrust value from the roll thrusters. High thrust valves are utilized during intermediate acquisition to quickly (about 4 seconds) provide a near-final value for roll position. This interval is characterized by high angular acceleration levels in the roll axis and low accelerations in pitch and yaw. During fine acquisition the maximum roll thrust level is reduced by a factor of 20 to conserve thruster gas (Freon 14). No sacrifice in performance occurs with the thrust level change since large values of acceleration are no longer needed during fine acquisition.

1.2 Fluidic Roll Control Loops

Figure 1 illustrates the integration of the fluidic roll control loops in SPARCS which would utilize a fluidic proportional thruster to modulate the roll (also pitch and yaw) thrusters. The interfacing logic required is relatively simple and would be implemented in electronics (with exception of the latching relay signal "L"

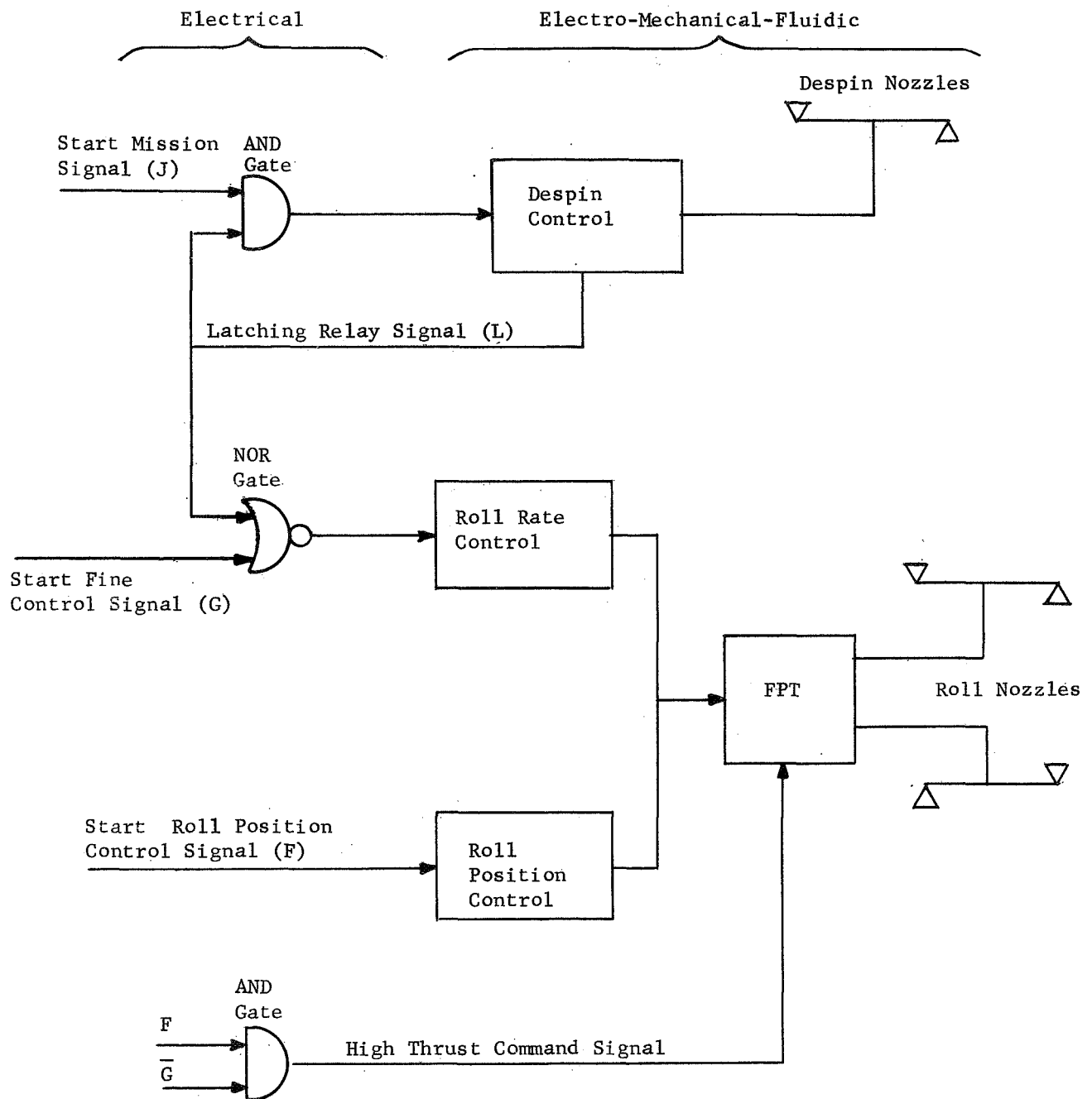*Solar Pointing Aerobee Rocket Control System

1

Fig. 1 Block Diagram - SPARCS Fluidic Roll Control.

2

which is described later in Section 2.0) and the electrical inter-
face signals (J, F and G) are available from the present control
system. A discussion of the operation of the required electrical
logic shown in Figure 1 is provided in Appendix II.

Figure 2 is a schematic illustrating the interconnection of the
roll control loops. Each of the loops (despin, roll rate, and
roll position) is initiated with a solenoid valve which applies
fluid power to the control loop. The despin loop drives despin
nozzles while the roll rate and roll position loops operate the
FPT which in turn operates the roll thrust nozzles. A single
vortex rate sensor is utilized first for the despin loop and later
for the roll rate loop during coarse acquisition. Vent flow from
the despin control is collected and utilized in the despin nozzles
as shown in Figure 2. Also as shown in the insert in Figure 2,
provision is made for collecting the vent flow from the fluidic
roll rate and roll-position control loops. The gas is collected
and exhausted through the vortex valves in the FPT to prevent
generation of random thrusts which would result if the vent flow
were simply dumped overboard. Typical supply pressures for the
various control components are listed in Figure 1. Detail descrip-
tion of the circuit design and performance are described for the
despin control, the roll rate control and the roll position control
in Sections 1.0, 2.0 and 3.0 respectively.

1.3 Conclusions and Recommendations

1. Accuracy of the roll position control exceeds that required
    in the current SPARCS system specification (+.1 deg) and
    power consumption is small. In most cases the gas used in
    the fluidic sensors and computing networks could also be
    used to provide reaction control torques. The primary
    disadvantage of the fluidic mechanization lies in the need
    to either physically align the magnetometer to a preset
    attitude prior to launch (and accept this inflexibility in
    launch plans) or employ a mechanical stepping motor to
    position the sensor as required. If the stepping motor
    were required, this would neutralize most of the benefits
    normally accruing with the use of fluidic devices
    (reliability, simplicity, etc) and it would be difficult
    to recommend the fluidic system over the current SPARCS
    electronic roll control.

2. The fluidic magnetometer, designed as a part of the roll
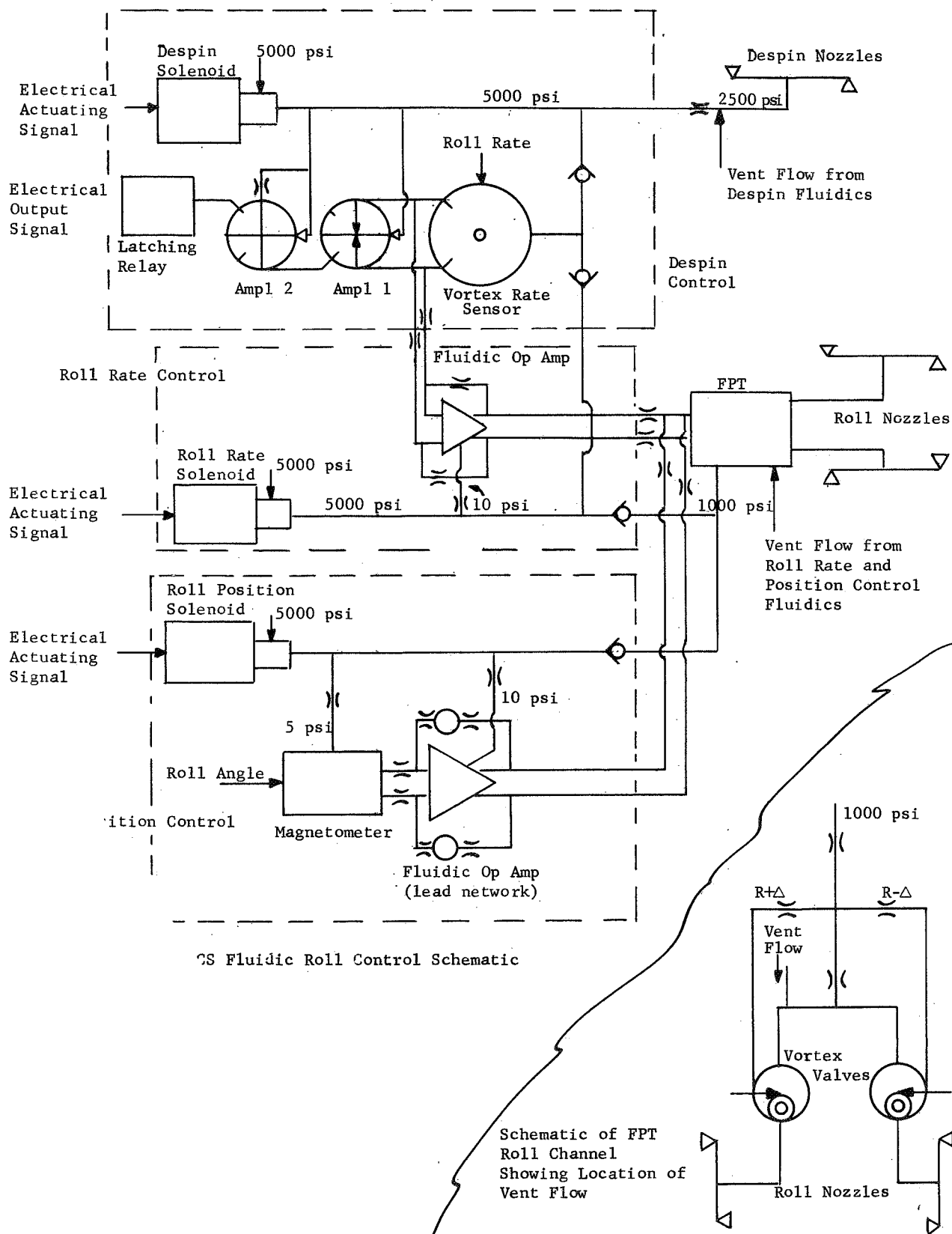   position control, appears to be a novel design and is the

Fig. 2 System Schematic - Fluidic Roll Control Loops.

4

only means known by the authors to generate a magnetic heading signal with fluidic devices. Additional applications other than the SPARCS mission could employ this heading reference; e.g.:

-- Simple attitude hold for astronauts during EVA missions (the complexity of the fluidic magnetometer being substantially less than that of an attitude gyro).

-- Emergency heading systems for aircraft and certain types of maneuverable and flyable ejection seats wherein electrical power is either not available or where a pneumatic output, at a significant power level, is desired for the sensor.

3. Fluidic implementation of the despin control is practical and provides the needed performance. The combination of a fluidic rate sensor and despin control valve could be packaged as an integral unit which can be simply interfaced with the existing SPARCS control system. The fluidic despin control is attractive since it eliminates relatively complex electronic computation for computing roll rates during despin. Because of the simplicity of interfacing and the integrated sensor/valve design, the despin control could be easily and economically phased into the current SPARCS package.

4. Fluidic implementation of the roll-rate control also is practical and can provide the needed performance. Use of the fluidic control again would eliminate the complex electronic computation of roll rate from the magnetometer signals. The power Freon consumption would be a small (less than 6%) compared to that needed for the total mission and the control circuitry could be easily interfaced with the present-design fluidic proportional thruster.

2.0 DESPIN CONTROL

The function of the despin control is to decrease large, initial roll rates to a value near zero. Figure 3 is a circuit diagram of the control. The vortex rate sensor and two amplifiers receive supply pressure from an electrically-operated solenoid valve. The rate sensor, amplifiers and a pneumatically-operated normally-closed latching-relay are enclosed in a pressure vessel which is initially maintained by means of orifice "A" and properly sized fluidic components at about 2500 psi for a supply pressure of 5000 psi. The pressure ratio across the sensor and amplifiers thus is maintained at about 2 to avoid supersonic pressure ratios across the fluidic elements.

The rate sensor is geometrically biased by rotating the sensor probe so that the output goes through zero at a rate of ten degrees per second as shown in Figure 4. Thus at zero roll-rate the rate-sensor output polarity is opposite the polarity existing when the vehicle is initially rolling.

The vortex rate-sensor output is amplified by the first of the two amplifiers following the sensor (Figure 3). The output of this amplifier is applied to one control port of amplifier 2 and the output of amplifier 2 drives the bellows actuated latching toggle switch.

In operation high initial roll rates provide a large positive ΔP output from the vortex rate sensor. This polarity signal applied to amplifier 2 aids the bias resistor in maintaining amplifier 2 output saturated in the "+" polarity and the output is simply vented. In this state pressure is applied to the despin thrusters to decrease roll rate. As roll rate passes through 10 deg/sec the output polarity from the rate sensor reverses and, as the roll rate approaches zero, signal pressure P1 at amplifier 2 is larger than bias pressure P2. As a result the output from amplifier 2 is now directed into the latching relay which interrupts flow to the despin nozzles thus ending despin control. Operating the sensor in this manner (geometrically biased) and using a bias on the output (second) amplifier prevents the possibility of false signals when the supply pressure is first turned on. (The rate sensor has a finite fill time and for a short period of time will have zero output even though it is rotating.)

The despin control is operated unregulated from the main supply of Freon 14 and supply pressure will drop during its operation. Moderate supply pressure changes will have little affect on despin control operation since all the fluidic devices including the bias resistor operate turbulent; i.e. they will obey square law pressure/ flow relationships and thus pressure ratios should remain nearly constant as the supply pressure drops. The gain of amplifier 1 and amplifier 2 will remain essentially constant since supply/vent pressure ratios are thus maintained constant. A properly designed system thus will be essentially independent of supply pressure changes.
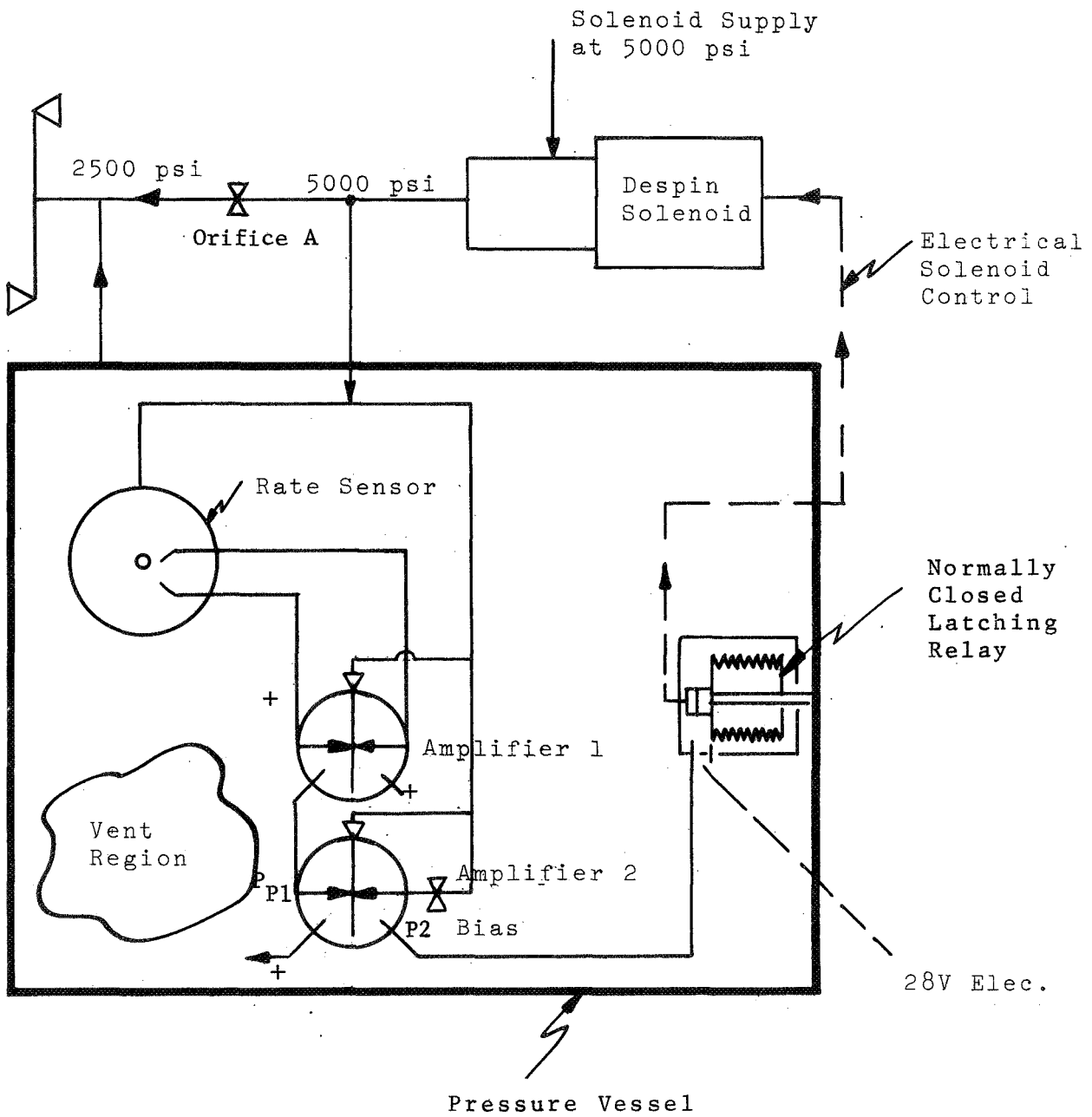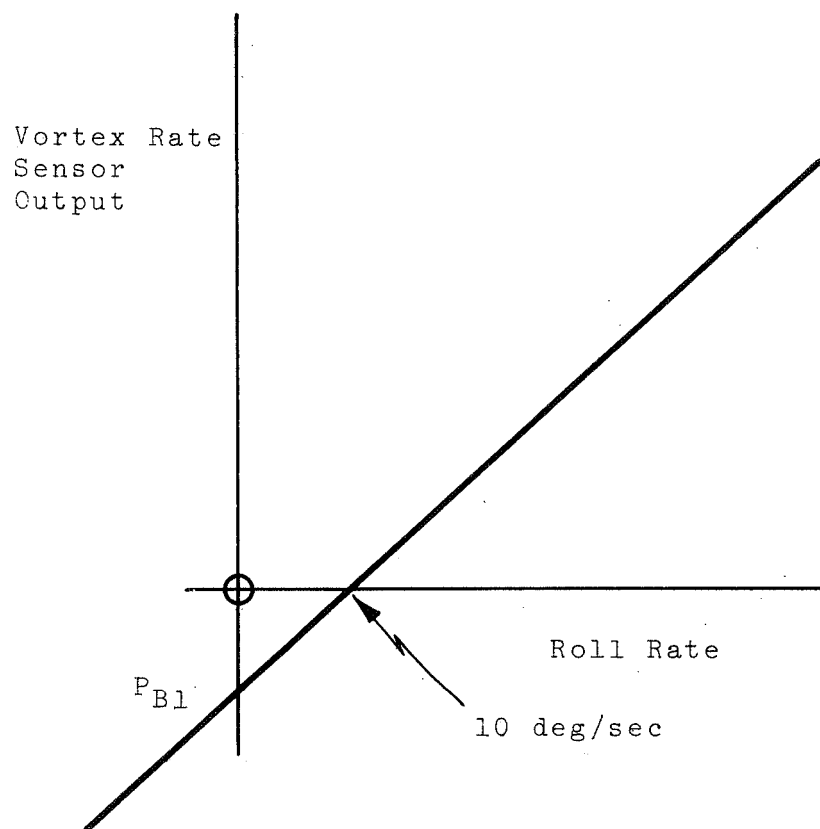
Fig. 3 Fluidic Despin Control.

Fig. 4 Vortex Rate Sensor Output vs Roll Rate.

The vortex rate sensor and its associated amplifiers require a Freon flow of about .008 lbm/sec and all this flow is utilized to produce useful reaction torques to despin the vehicle. Over 90% of reaction torque is supplied by direct flow from the despin valve through the orifice A shown in Figure 3. For a despin which requires eight seconds to complete (a very long despin time for a typical SPARCS mission) the amount of Freon required is given by:

$$W_{Freon} = .008 \; \frac{lbm}{sec} \; x \; 8 \; sec = .064 \; lbm$$

A SPARCS mission should use a total of no more than about 5.8 lbm of Freon. Therefore, the amount of Freon required by the fluidics during despin is only .064/5.8 = 1.1 percent of the total amount allowed for a SPARCS mission.

The vortex rate sensor is the largest of the fluidic components. A commercially available unit occupies a space envelope which is 6.125 inches in diameter by 1.875 inches high. It is constructed from aluminum and weighs two pounds. The fluidic amplifiers employed would have a power nozzle cross section of .02 x .02 in. Restrictor A must have an area roughly one-half the equivalent throat area of the despin nozzles. Two nozzles with a .067 inch throat diameter produce the despin couple. If orifice A were sized at .067 inch diameter, then its area would be half the total nozzle throat area. In addition, though, a discharge coefficient in the neighborhood of 0.7 should be assumed to apply to orifice A. The diameter of orifice A then is:

$$\text{Dia orifice A} = \frac{.067 \; in}{\sqrt{.7}} = 0.080 \; inch$$

The despin control is attractive because it eliminates the necessity for electronically computing roll-rate from electrical magnetometers and sun sensors. The elimination of the electrical roll rate circuitry could result in about a 20% reduction in electronics. Before eliminating the electronic roll-rate circuitry some means must be devised for correctly interpreting the magneto-meter sinusoidal output. For example, the sine of a roll angle between -90 and +90 degree has positive slope, but the slope is negative in the other two roll angle quadrants. A roll rate computation will take on a polarity which depends on the slope of the sine. Therefore, a position control which is rate damped and derives all position and rate information from a magnetometer sinusoidal output alone can only be stable in two of the four roll angle quadrants. Further effort is needed to resolve this deficiency.

3.0 COARSE ACQUISITION (Roll Rate Control)

The SPARCS coarse acquisition is the control phase during which large pitch and yaw errors are reduced to a small value (less than ten degrees). During coarse acquisition roll rate is held as close to zero as is possible. This results in the decoupling of the pitch and yaw control position loops which simplifies the control problem.

Figure 5 shows the roll rate control implementation. The loop is set up to command a zero roll rate. The moment arm and vehicle moment of inertia are typical of those for SPARCS inserts launched by Aerobee 150 sounding rockets. The fluidic proportional thruster (FPT) is similar to one being built for NASA/ARC under contract NAS 2-5466 with the exception that the input command is a differ-ential pressure instead of a voltage. The vortex rate sensor is the same one considered in Section 2.0 for despin control.

The vortex rate sensor scale factor applies to operation on Freon 14 and is about a factor of three greater than for air operation since Freon density is three times that of air. The operational amplifier closed-loop gain of 20.6 is a reasonable value to implement, and it is low enough to prevent the amplifier from being too susceptible to null offsets at the input.

An open loop gain of unity in Figure 5 produces a closed loop transfer function given approximately by:

$$\frac{\delta \dot\phi}{\delta \dot\phi_c} = \frac{58.9}{1 + S} \quad \frac{deg/sec}{psi}$$

As the equation shows, the roll rate control response to a small signal command is about one second. This appears adequate for SPARCS coarse control roll-rate control requirements.

The fluidic elements required for roll rate control are the vortex rate sensor, operational amplifier and the FPT. The FPT provides the power for roll, pitch and yaw control during coarse, intermediate and fine acquisitions. Its size should not be charged against the roll-rate control portion of coarse acquisition because it must meet requirements which are independent of control signal implemen-tation (i.e. fluidic or electronic). The vortex rate sensor is the same as that used for despin (Section 2.0). Therefore, the only additional fluidic device required for roll rate control is the operational amplifier. The operational amplifier space requirement is about 2.0 cubic inches.

Dynamics

$$\frac{1}{S}$$

$\delta\dot\phi$ $\dfrac{deg}{sec}$

Vehicle

$$\frac{57.3}{4/3}$$

$\ddot\phi$ $\dfrac{deg}{sec^2}$

Moment Arm

$$\frac{2}{3}$$

ft-lb

FPT

$$\frac{.1}{1 + \frac{S}{20}}$$

lb

Operational Amplifier

$$20.6$$

psid

Vortex Rate Sensor

$$\frac{1.7\times10^{-2}\,\varepsilon - .01S}{1 + \frac{S}{90}}$$

psi

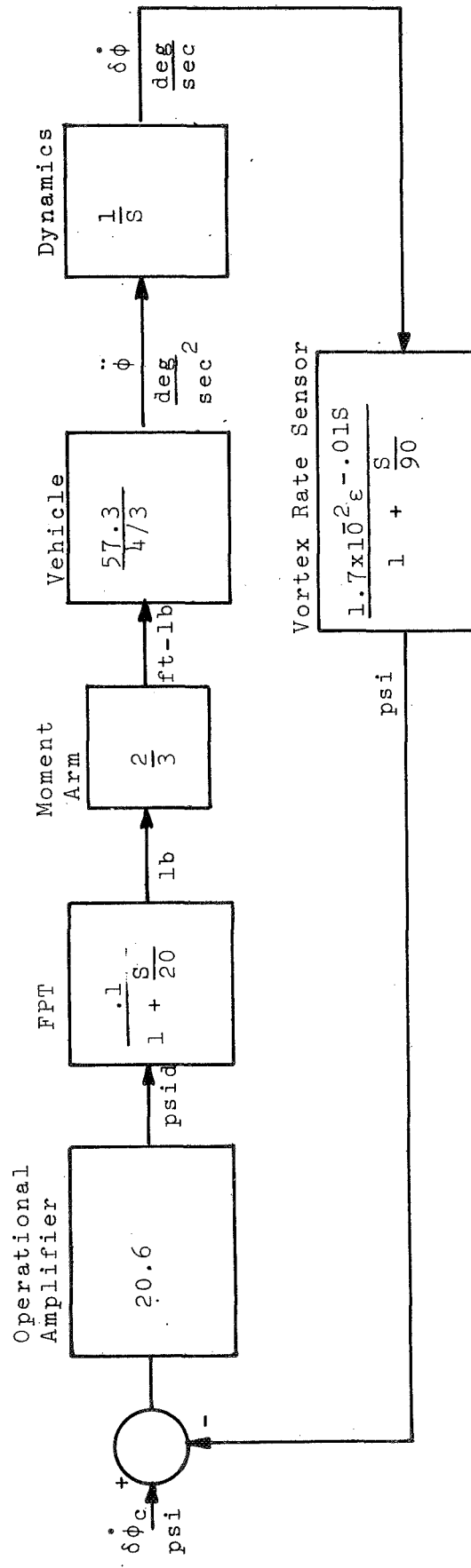$\delta\dot\phi c$ psi   +   −

Fig. 5   Roll Rate Control Loop.

11

The flow required to drive the vortex rate sensor and operational
amplifier is estimated to be about the same as for despin; i.e.,
.008 lbm/sec. This flow is required through intermediate control up
to the time the fine control begins. The need for some roll rate
control during the roll positioning of the vehicle during intermediate
acquisition is caused by the inability to derive accurate roll rate
information from the time derivative of magnetometers. This is a
problem only for certain magnetometer orientations which are not
encountered in fine acquisition. The total time required to finish
the coarse and intermediate acquisition phases should not
exceed 40 seconds. Therefore, the amount of Freon required is:

$$W = 0.008 \ \frac{lbm}{sec} \ x \ 40 \ sec = 0.32 \ lbm$$

Assuming, as in Section 2.0, that 5.8 lbm of Freon can be applied
for an entire SPARCS mission, then .32/5.8 = 5.5% of the usable
Freon is required for generating roll control signals in despin,
coarse and intermediate acquisition. This flow for operation of
the fluidic circuitry is captured and vented through the FPT, thus
impulse is obtained from this gas consumption.

4.0 ROLL POSITION CONTROL (Intermediate and Fine Acquisition)

The fluidic roll position control, shown in block diagram form in Figure 6, is a relatively conventional control approach, but it utilizes all fluidic components to perform the sensing and compensation thrust-modulation functions. The position loop shown in Figure 6 is for fine acquisition. During intermediate control the loop must be slightly modified by adding pure rate feedback from a rate sensor such as the one described in Section 3.0. This is necessary to overcome possible erroneous rate signals which are generated by the pseudo differentiation of the magnetometer output by the lead portion of the fluidic compensation. The key component in the roll position loop is the magnetometer. Hence, most of the effort in this study was directed at this device.

4.1 Magnetometer

The function of the fluidic magnetometer is to deliver a differential output pressure signal which is proportional to the angle the magnetometer makes with the earth's magnetic field. It differs from the conventional magnetometer by delivering a pneumatic output instead of an electrical output.

A sketch of the magnetometer is shown in Figure 7 and a schematic in Figure 8. The sensing element is an Alnico 5 bar magnet mounted on a flexpivot to permit angular displacement about the sensitive axis. A jet pipe attached to the magnet assembly directs a jet at two receivers located in the base plate. Angular displacement of the jet pipe relative to the receivers results in a differential pressure-signal which is amplified and applied as a nulling torque on the assembly. The fluidic amplification includes a signal amplifier, a lead-lag and an output amplifier. The lead-lag provides loop stabilization; its operation is described in Appendix III. The output of the magnetometer is the differential pressure across the torquing nozzles.

4.1.1 General Features and Characteristics

The estimated package size is 1.7 inches long by 1 inch wide and 3/4 inches high; the weight is 0.1 lb. The assembly requires a supply air flow of 4×10^4 lb_m/sec for a 5 psig supply pressure. The air volume-flow is given by:

$$Q = \dot{W} \frac{RT}{P} = 4 \times 10^{-4} \frac{lb_m}{sec} \times 639 \frac{in\text{-}lb}{lb_m\,{}^\circ R} \times \frac{530\,{}^\circ R}{(14.7+5)\,lb/in^2} \qquad (1)$$

$$Q = 6.9 \ in^3/sec \quad air \ flow$$
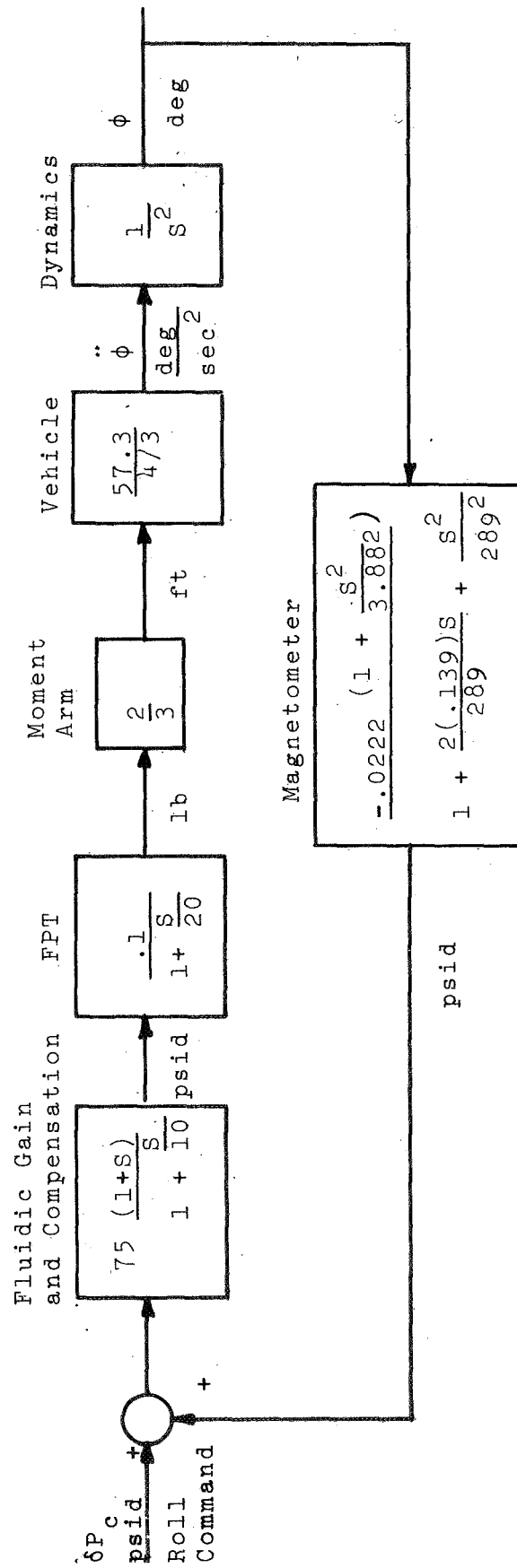
13·

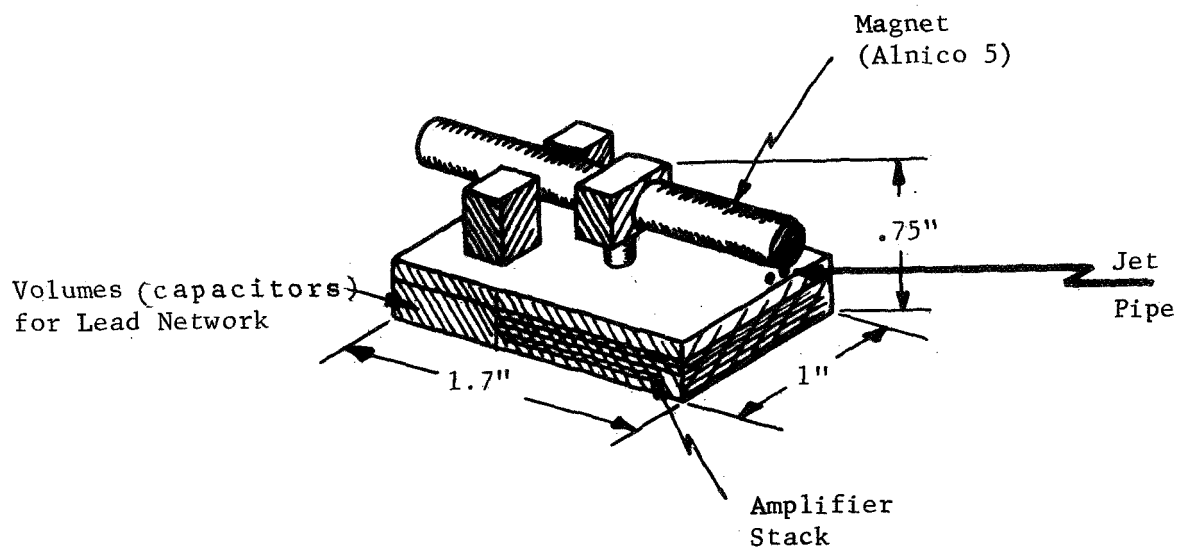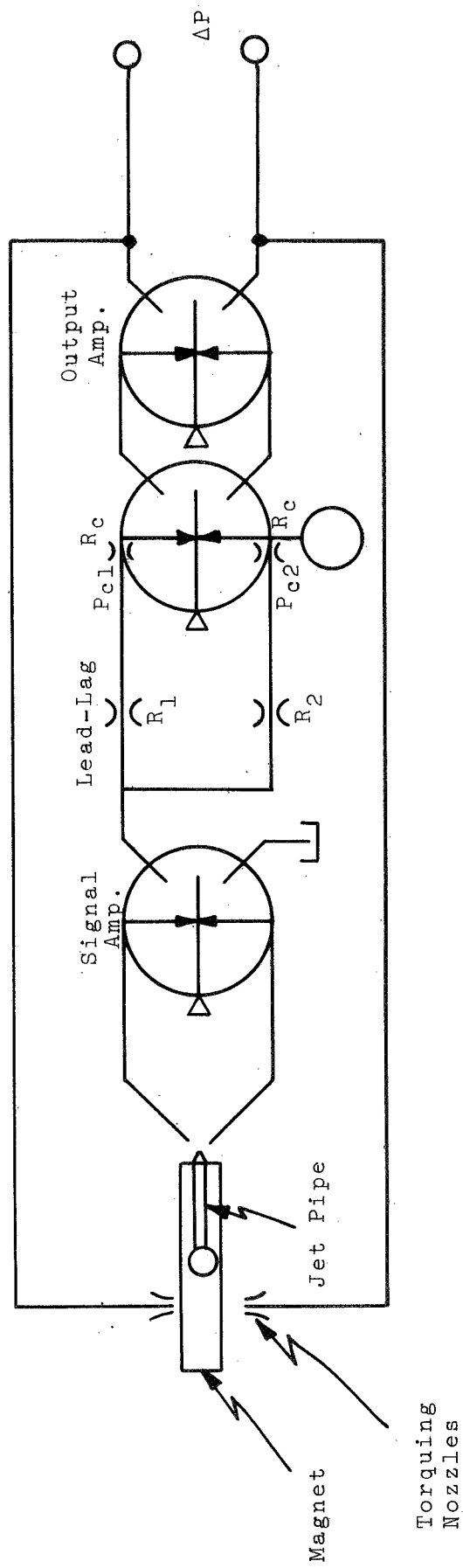Fig. 6 Roll Position Control Loop.

14

Fig. 7 Magnetometer.

15

Fig. 8 Magnetometer Schematic.

16

The power consumption of the magnetometer is:

$$\text{Power} = Q\,p = 6.9 \ \frac{\text{in}^3}{\text{sec}} \ \text{x} \ (14.7+5) \ \frac{\text{lb}}{\text{in}^2} = 135 \ \frac{\text{in-lb}}{\text{sec}} = 15.3 \ \text{watts} \qquad (2)$$

If the magnetometer is operated on Freon 14, different values result for the mass and volume flows and hence the power consumption is altered. The supply pressure and the orifice areas in the magnetometer can be the same for Freon as for air and the Freon 14 mass flow is approximately

$$\dot{W}_{\text{Freon}} \approx \sqrt{\frac{\text{Freon 14 molecular weight}}{\text{Air molecular weight}}} \ \text{x} \ \dot{W}_{\text{air}} = \sqrt{\frac{88}{29}} \ 4\text{x}10^{-4} \ \frac{\text{lbm}}{\text{sec}} \qquad (3)$$

$$\dot{W}_{\text{Freon}} \approx 7 \ \text{x} \ 10^{-4} \ \text{lbm/sec}$$

Assuming that Freon 14 is an ideal gas, the volume flow is given by

$$Q_{\text{Freon}} = \frac{\dot{W}_{\text{Freon}} R_{\text{Freon}}}{p} \ T = 7\text{x}10^{-4} \ \frac{\text{lbm}}{\text{sec}} \ \text{x} \ 208 \ \frac{\text{in-lb}}{\text{lbm}^\circ\text{R}} \ \frac{530^\circ\text{R}}{(14.7+5)} \ \text{lb/in}^2$$

$$= 3.92 \ \frac{\text{in}^3}{\text{sec}} \qquad (4)$$

and the power delivered by the regulated Freon 14 supply is

$$\text{Power} = Qp = 3.92 \ \frac{\text{in}^3}{\text{sec}} \ \text{x} \ (14.7+5) \ \frac{\text{lb}}{\text{in}^2} = 77.3 \ \frac{\text{in-lb}}{\text{sec}} = 8.7 \ \text{watt} \qquad (5)$$

The above expressions reveal that a higher molecular-weight gas, such as Freon 14, operates the magnetometer with a lower power consumption even though the mass flow of Freon 14 exceeds that of air.

Current SPARCS missions last three hundred seconds and use Freon 14 to power an on-off thruster control system. The total mass of Freon 14 required for a mission (allowing for a reasonable reserve of thirty percent in the tank at the end of the mission) is 4.7 lbm. The total mass of Freon 14 required to operate the magnetometer is given by

$$300 \ \text{sec x} \ 7 \ \text{x} \ 10^{-4} \ \text{lb/sec} = 0.21 \ \text{lbm}$$

4.1.2 Magnetometer System Analysis

Figure 9 shows the coordinate system used to determine the displacement of the magnetometer magnet with respect to both the magnetometer frame and the earth's magnetic field. The angle ϕ is the roll angle which the magnetometer frame makes with the earth's magnetic field and is the angle which the magnetometer measures. The angle ϕ_r is the angular displacement of the magnet with respect to the magnetometer frame. The magnet is mounted on a flexpivot which develops a restoring torque given by

$$T_{flexpivot} = -K_r \phi_r \qquad (6)$$

$$K_r = .01 \text{ in-lb/rad} = 1.75 \times 10^{-4} \text{ in-lb/deg}$$

A second torque on the magnet is caused by the interaction of the magnet's flux with the earth's magnetic field and is identified as magnetic torque.[1] The relation between this magnetic torque and ϕ_m, the angle from the earth's magnetic field to the magnet's axis, is obtained using the geometry illustrated in Figure 10.

The couple exerted on the magnet is $F \times L_m$ where the force, F, is given by

$$F = -m H \sin \phi_m \sin \eta \qquad (7)$$

The torque, τ, then becomes

$$\tau = -m H L_m \sin \phi_m \sin \eta \qquad (8)$$

where:
η = angle between sun line vector and earth's magnetic field
$H \approx 44$ amp/meter earth's magnetic field
m = pole strength in units of magnetic flux (webers)
$L_m = (1.6 \text{ in}) \times .7 = 1.12 \text{ in} = .0285$ meter equivalent magnet length

The pole strength is defined as the magnetic flux at the end of the magnet and is given approximately as the product of the flux density of the magnet with the magnet's face area. The magnet characteristics considered for the magnetometer are that of an Alnico 5 cylinder 0.25 inches in diameter by 1.6 inches long. An Alnico 5 magnet can be magnetized to a flux density of 1.25 webers per square meter. Therefore, the pole strength of the magnet is given by

[1] *Electricity and Magnetism*, Francis Weston Sears, Addison-Wesley Publishing Company, 1946.

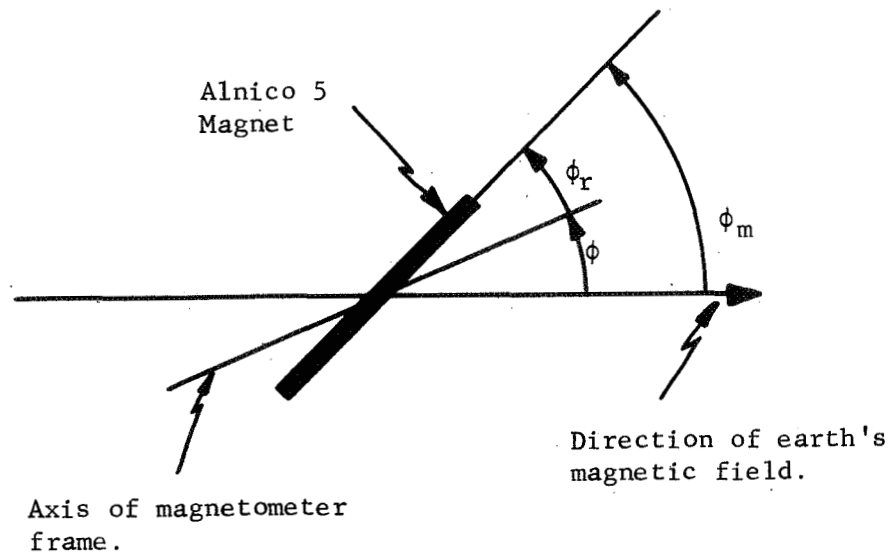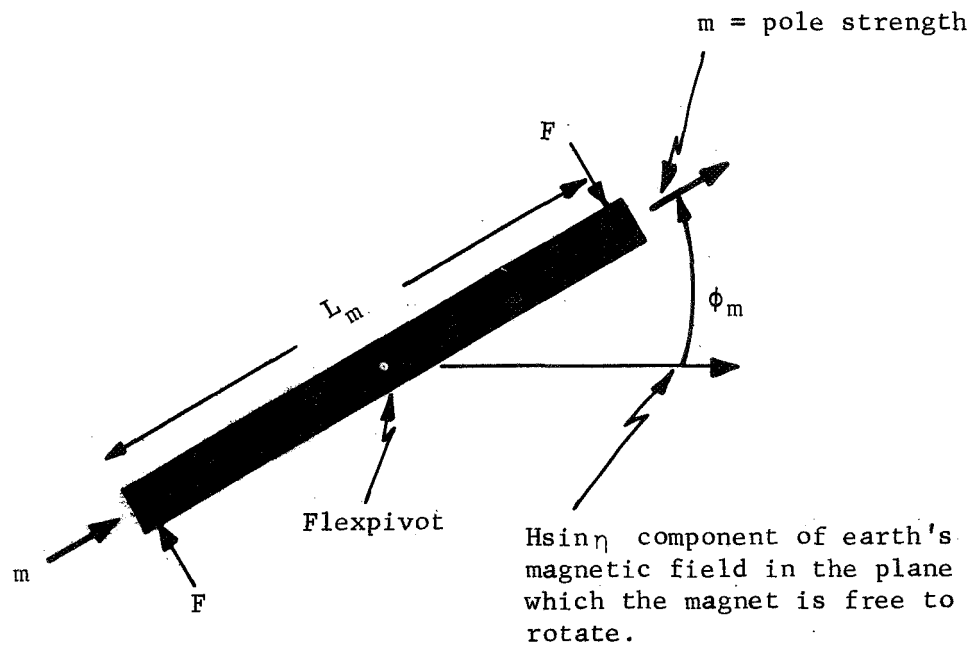Fig. 9 Magnetometer Coordinate System.

m = pole strength

F

L_m

ϕ_m

Flexpivot

$H\sin\eta$ component of earth's magnetic field in the plane which the magnet is free to rotate.

m

F

Fig. 10 Schematic for Electro-Mechanical Interactions.

20

$$m = BA = 1.25 \; \frac{\text{webers}}{\text{meter}^2} \; x \; \frac{\pi}{4} \; (.25)^2 \; \text{in}^2 \; x \; \frac{1 \quad \text{meter}^2}{1548 \; \text{in}^2} = 3.96 \times 10^{-5} \; \text{webers}$$ (9)

Substituting numerical values into (8) provides an estimate of the magnetic torque for the magnet under consideration; i.e.

$$\tau = mHL_m \sin\phi \sin\eta = (3.96 \times 10^{-5} \; \text{webers} \; x \; 44 \frac{\text{amp}}{\text{meter}} \; x \; .0285 \text{meter}) \sin\phi \sin\eta$$

$$\tau = 4.96 \times 10^{-5} \sin\phi \sin\eta \; \text{weber amp} = 4.96 \times 10^{-5} \sin\phi \sin\eta \; \text{newton-meter}$$

or equivalently

$$\tau = -4.39 \times 10^{-4} \sin\phi \sin\eta \quad \text{in-lb}$$ (10)

The incremental change in the magnetic torque with roll angel, ϕ, is an important value in the control analysis. This value is given by

$$\delta\tau = \frac{\partial\tau}{\partial\phi} \; \delta\phi = -K_m \; \delta\phi$$

where a delta, δ, indicates an increment in the variable (11)

$$K_m = \frac{\partial\tau}{\partial\phi} = 4.39 \times 10^{-4} \cos\phi \; \sin\eta \; \frac{\text{in-lb}}{\text{radian}}$$

The maximum value of K_m is 4.39×10^{-4} in-lb/radian and occurs if $\phi = 0$ and $\eta = 90$ degrees. For other values of ϕ and η, the magnitude of K_m decreases. For η less than zero the sin is negative and K_m is negative which, in some cases, can cause instability which also occurs in the present electronic magnetometer. This condition is avoided by selected launch times to provide faborable sun position.

In addition to the flexpivot restoring-torque and the magnetic torque a third restoring torque is applied to the magnet by the fluidic circuit and here is identified as the nulling torque. The nulling torque is caused by a differential pressure applied to an area, A_c, at a distance, L_c, from the pivot. For the Alnico 5 magnet being considered the area and length are:

$$A_c = \frac{\pi}{4} (.02 \; \text{in})^2 = \pi \; x \; 10^{-4} \; \text{in}^2$$

$$L_c = 0.5 \; \text{in}$$ (12)

$$L_c A_c = 1.57 \times 10^{-4} \; \text{in}^3$$

The moment of inertia of the cylindrical magnet is I_m and is computed as follows:

$$I_m = M_m \left[\frac{(L_m)^2}{12} + \frac{(D_m)^2}{4} \right] \qquad (13)$$

$$M_m = 2.05 \times 10^{-2} \text{ lbm} = 5.33 \times 10^{-5} \frac{\text{lb-sec}^2}{\text{in}}$$

Then:

$$I_m = 5.33 \times 10^{-5} \frac{\text{lb-sec}^2}{\text{in}} \left[\frac{(1.6\text{in})^2}{12} + \frac{(.25\text{in})^2}{4} \right] = 1.22 \times 10^{-5} \text{ in-lb sec}^2$$

The gain of the jet pipe, which drives the first stage of the fluidic circuitry, is computed as follows: assume a relative jet-pipe displacement of 0.010 inch from null is sufficient to drive the output of the first amplifier into a saturation of 0.5 psi. If the jet pipe is at the end of 1.6 inch Alnico 5 magnet, then the angle ϕ_r which corresponds to a 0.010 inch displacement is:

$$\phi_r = \frac{0.010 \text{ in rad}}{(1.6/2) \text{ in}} = 1.25 \times 10^{-2} \text{ radian}$$

Since this angle drives the first amplifier output to 0.5 psi, the jet pipe gain is approximately

$$K_j \approx \frac{0.5 \text{ psi}}{\phi_r} = \frac{0.5 \text{ psi}}{1.25 \times 10^{-2} \text{ radian}} = 40 \frac{\text{psi}}{\text{radian}} \qquad (14)$$

With all the torques which are applied to the magnet determined and the moment of inertia of the magnet identified, a small-signal block diagram of the magnetometer can be drawn. This is shown in Figure 11 where a delta, δ, denotes an incremental value of the variables. All torques sum at the input to the magnet; these torques divided by the moment of inertia of the magnet produce an inertial angular acceleration, $\delta\ddot{\phi}_m$. The double integration of the inertial acceleration produces the inertial angle $\delta\phi_m$. This angle, $\delta\phi_m$, times K_m produces the magnetic restoring torque, $\delta\tau$. The roll angle of the magnetometer frame, $\delta\phi$, subtracted from $\delta\phi_m$ is the relative displacement, $\delta\phi_r$. The flexpivot restoring torque is equal to the relative displacement times K_r. The relative displacement is also sensed by the jet pipe-receiver assembly and converted by fluidic amplifiers to a differential pressure, δP. The differential signal pressure, δP, times $L_c A_c$ becomes the nulling torque. The lead network is necessary to stabilize the loop since the loop contains a double integration.
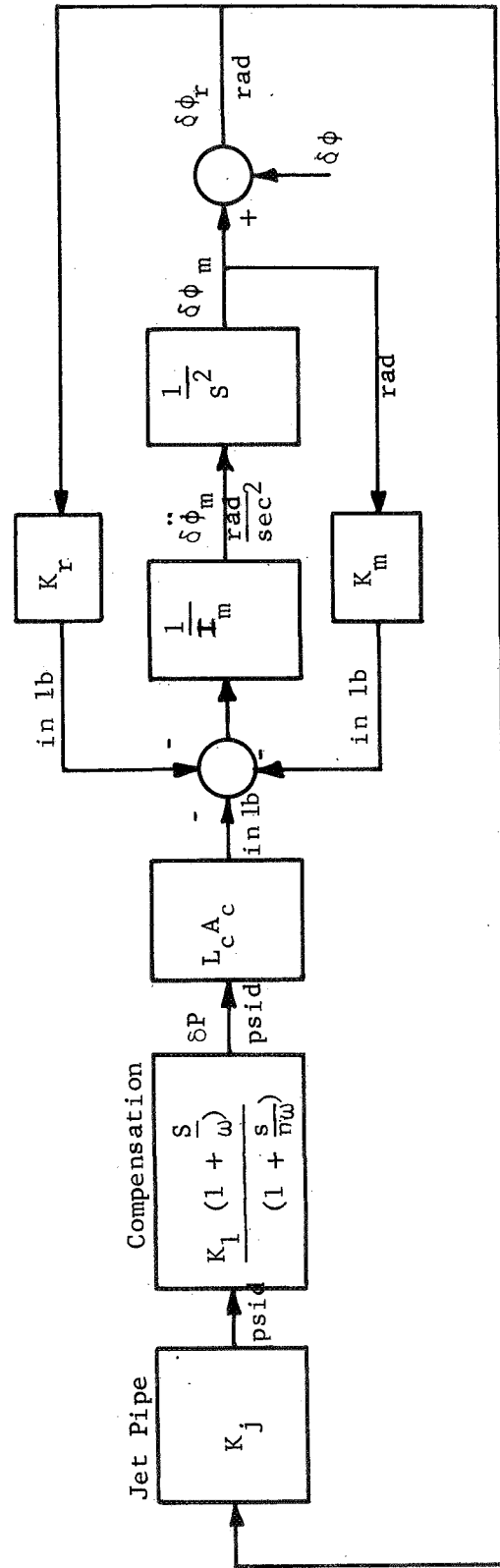
22

Fig. 11 Magnetometer Small Signal Block Diagram.

The behavior of δP vs $\delta\phi$ is fundamental relationship which is of primary interest. The small-signal block diagram of Figure 5 can be reduced to the form in Figure 10. As shown, the open loop phase lag will not exceed 180 degrees unless the value of "n" is less than unity. For values of "n" less than unity though, the compensation becomes a lag-lead rather than a lead network. Therefore, the closed loop of Figure 11 will always be stable if a lead compensation network is used. In reality higher order lags always are present in a system so there will be some frequency at which the open loop phase lag exceeds 180 degrees for n greater than unity. The gain at that frequency must not exceed unity if the loop is to be stable.

Values from equations (6), (11), (12), (13), and (14) when substituted in the small signal block diagram (Figure 12) results in the diagram shown in Figure 13. The ratio of the lag to the lead break frequency in the lead network is ten, a readily attainable value. The geometric mean of the lead and lag frequencies in the lead network where maximum phase lead occurs is about 28.6 radians/ second, the frequency where the open loop gain becomes infinity. In reality the gain at this point will be finite because some damping is always present and the phase lag remains less than 180 degrees as a result of the compensating effect of the lead network. The required gain of the amplifiers following the jet pipe amplifier is established at 16.6 psid per psid. This value can be easily developed by two fluidic amplifiers and provides a low-frequency open-loop gain of ten.

4.1.3 Magnetometer Closed Loop Performance

The magnetometer closed-loop performance has been calculated for three different values of $\cos\phi\sin\eta$. The closed loop behavior is based on the block diagram values shown in Figure 13. For convenience here the scale factor is expressed in psid* per degree instead of psid per radian. The results are:

For $\cos\phi\sin\eta = 1.0$ (e.g. $\phi = 0$ deg; $\eta = 90$ deg)

$$\frac{\delta P}{\delta \phi} \approx \frac{-.0444 \quad (1 + \frac{s^2}{7.75^2})}{1 + \frac{2(.14)S}{286} + \frac{s^2}{(286)^2}} \quad \frac{psid}{deg} \tag{15}$$

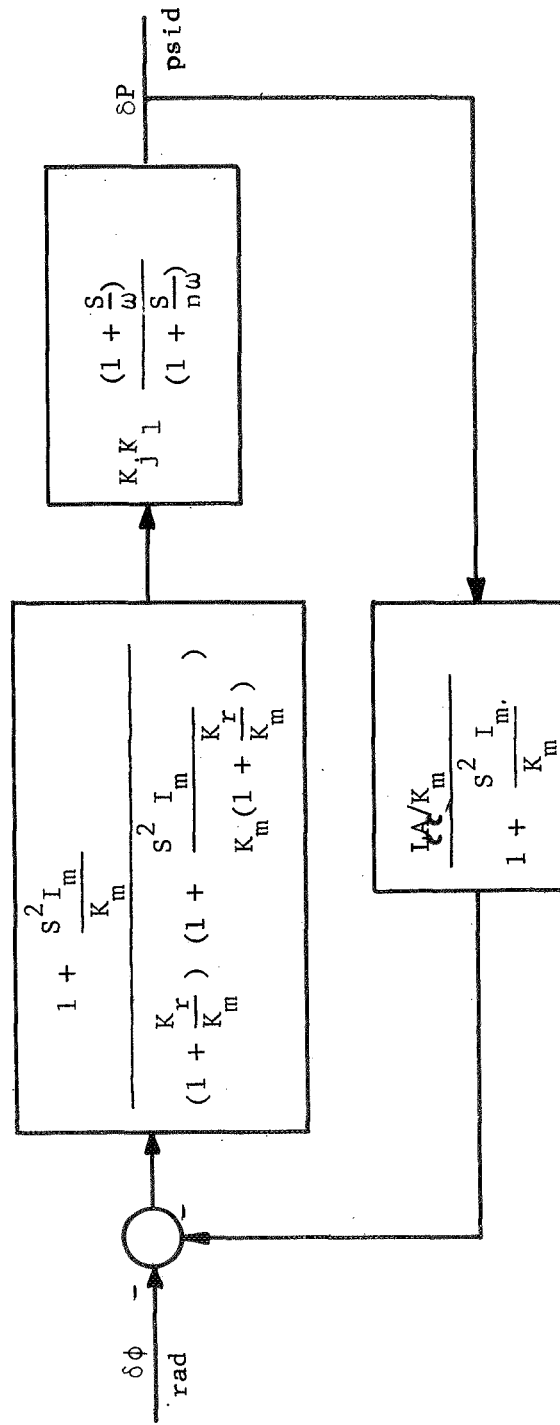*differential pressure in-(lb/in^2)

Fig. 12 Reduced Magnetometer Small Signal Block Diagram.
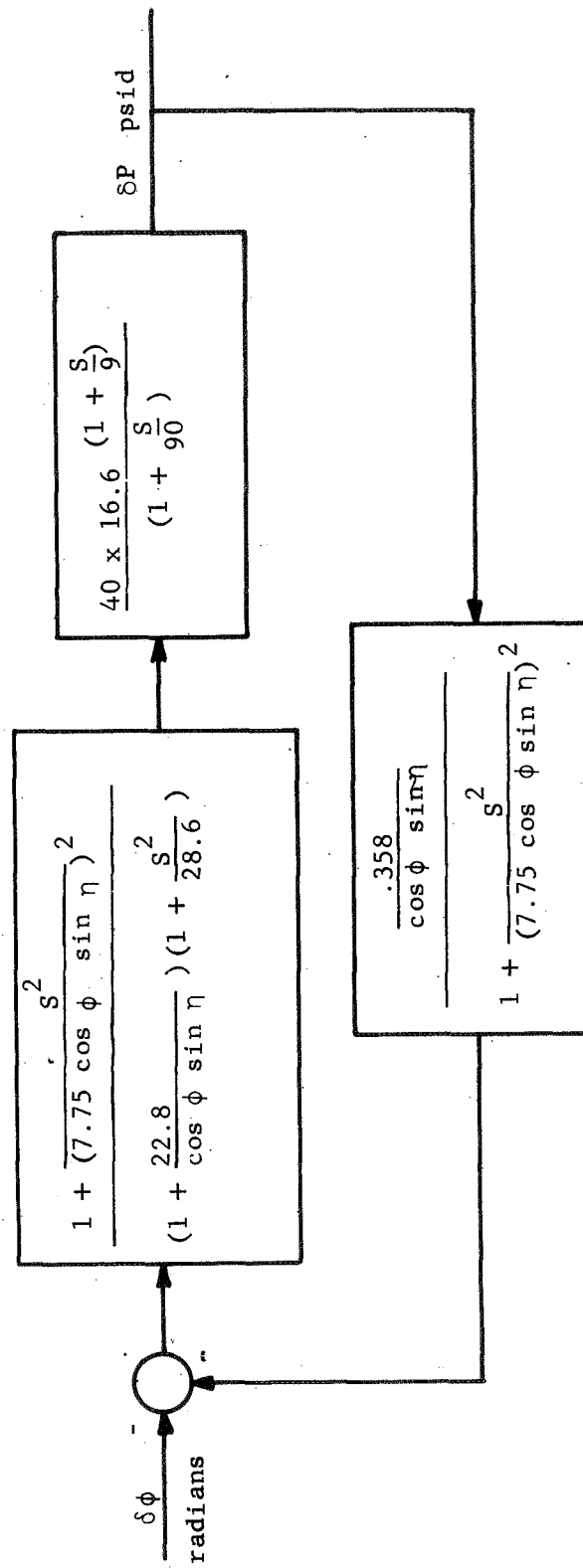
25

Fig. 13 Magnetometer Small Signal Block Diagram with Numbers.

26

For cosϕsinη = 0.5 (e.g. ϕ = 45 deg; η = 45 deg)

$$\frac{\delta P}{\delta \phi} \quad -.0222 \frac{(1 + \frac{s^2}{3.88^2})}{1 + \frac{2(.139)S}{289} + \frac{s^2}{(289)^2}} \quad \frac{psid}{deg} \tag{16}$$

For cosϕsinη = 0.0301 (e.g. ϕ = 80 deg; η = 10 deg)

$$\frac{\delta P}{\delta \phi} \cdot -.00134 \frac{(1 + \frac{s^2}{.233^2})}{1 + \frac{2(.137)S}{293} + \frac{s^2}{(293)^2}} \quad \frac{psid}{deg} \tag{17}$$

The primary source of noise in the magnetometer is in the jet pipe and the fluidic compensation. The spectral density of this noise was estimated from previous noise tests at G.E. Using standard control techniques these noise sources can be combined and moved outside the magnetometer loop. The resulting spectral density has a value of 10^4 deg^2/Hz. If the magnetometer is used in a position control loop whose low pass bandwidth is 1 Hz, then the rms position uncertainty is 0.01 deg which is adequate for a SPARCS mission.

Equations (15), (16) and (17) show the scale factor and second-order lead break-frequency to change substantially with cosϕsinη (i.e. with the spatial position of the magnetometer). The ratio of the change in the scale factor is nearly identical with the change in the second-order lead break frequency. Variations in these values are of concern when the magnetometer is employed as a component in a control loop. The denominator of the closed loop transfer function (Eq. 15, 16, 17) is a lightly-damped, second-order term which does not change significantly with the spatial position. The natural frequency is about 289 radians per second (46 Hz) and although the damping ratio is low ($\approx$ .139), good closed-loop performance can be obtained as discussed in paragraph 4.2.

Loop stability could be much easier achieved if the second-order lead were far beyond the loop crossover frequency. The lead-break can be made to occur at a higher frequency but at a great sacrifice in magnetometer sensitivity as shown as follows. The second-order

break frequency in equations (15), (16), and (17) is

$$\text{Second-order break frequency} = \sqrt{\frac{K_m}{I_m}} \qquad (18)$$

If the form factor of the magnet is constant, then the moment of inertia, I_m, is proportional to the length raised to the fifth power. The magnetic spring constant, K_m, is proportional to length times pole strength. With a constant form-factor, the pole strength changes as the square of the length and K_m changes as the cube of the length. Therefore, the net change in the second-order lead with length is proportional to the reciprocal of the length. That is, halving the magnet's length will double the second-order lead frequency. Sensitivity is sacrificed however since, for a fixed form factor, the sensitivity changes as the reciprocal of the cube of the length. For example, halving the length decreases the sensitivity by a factor of 1/8. Therefore, reducing the size of the magnet to increase the second order break frequency is done at a great sacrifice in sensitivity.

At this point it is appropriate to point out that the approach applied to the design of the fluidic magnetometer could be adopted to an entirely electro-mechanical magnetometer. Rather than using pneumatics to develop nulling torques, a torque motor or similar electro-mechanical device would be used to produce them. Lead compensation would be provided by using an electronic operational amplifier. Additional compensation such as a lag network to provide higher low frequency gain could be implemented more easily with electronic instead of fluidic components.

4.2 Roll Position Closed Loop Performance

The roll-position control loop consists of a fluidic proportional thruster (FPT) for providing thrust, a roll moment-arm, the Aerobee 150 moment of inertia, the fluidic magnetometer (discussed in the previous section) and fluidic compensation to provide loop stability. The arrangement of these components in the control loop is shown in Figure 6. The FPT and Aerobee 150 transfer functions are nominal values. The magnetometer transfer function is that of equation (16) and applies for the condition of $\cos\phi\sin\eta = 0.5$.

The fluidic circuit schematic for the roll position compensation is shown in Figure 14. A standard fluidic operational-amplifier is used to provide the lead-lag characteristics. This amplifier is followed by two proportional amplifiers which provide the additional gain required in the loop and provide the power output to position the flapper-nozzle at the FPT input.
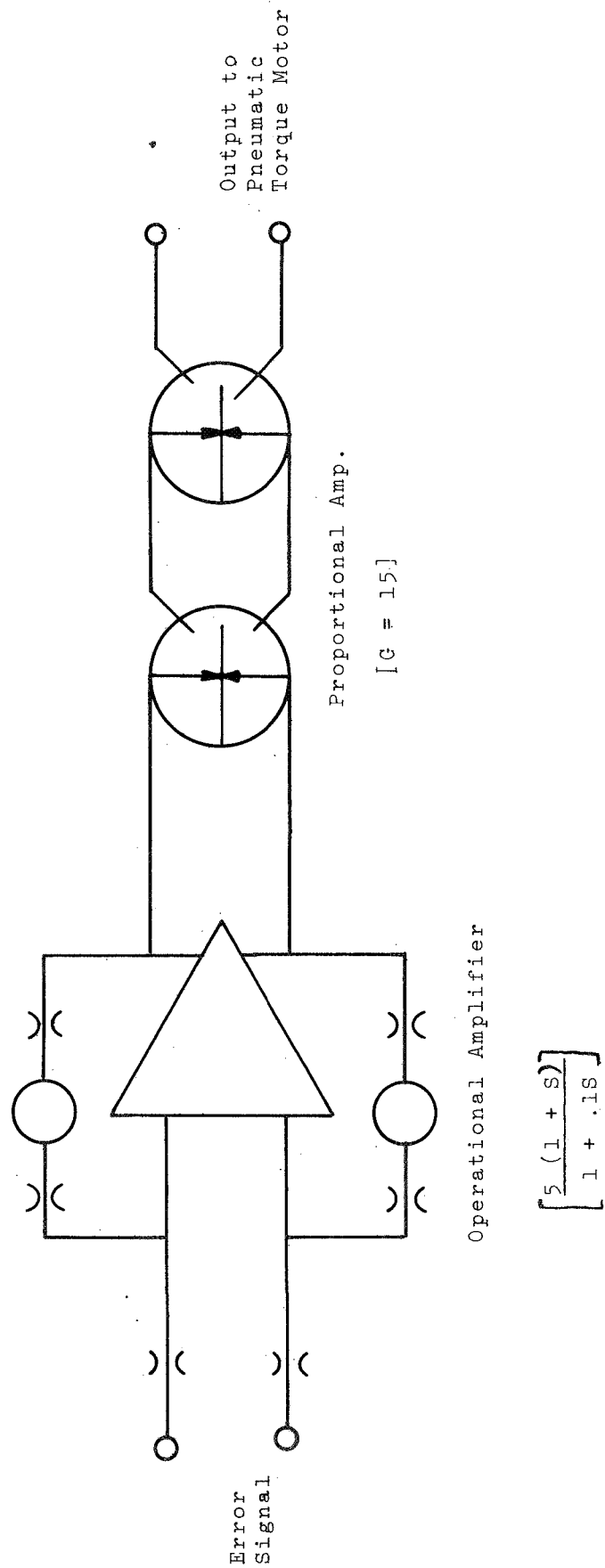
Fig. 14 Circuit Schematic Roll Position Compensation.

The total number of proportional amplifiers required in the position control is five (i.e. two for roll compensation plus three for the magnetometer). In addition, one operational amplifier is required for the roll compensation. The estimated air flow required by the five proportional and one operational amplifier is 7×10^{-4} lbm/sec. The power consumption (with air) is 26.8 watts. If Freon 14 is the operating fluid, the flow and power requirements are 12.3×10^{-4} lbm/sec and 15.2 watts respectively.

The total mass of Freon 14 required for a typical 300 second position control is:

$$W = 12.3 \times 10^{-4} \, \frac{lbm}{sec} \times 300 \, sec = .37 \, lbm$$

This is the mass of gas required to drive all the fluidic elements (including the magnetometer) in the roll position loop. Assuming, as in Section 2.0, that 5.8 lbm of Freon is disposable during the entire mission, then $.37/5.8 = 6.4\%$ of the usable Freon is required for roll position control.

The roll signal processing Freon gas requirement can be summarized as follows.

1.	Despin (Section 2.0)	0.064 lbm
2.	Coarse and Intermediate (Section 3.0)	0.32 lbm
3.	Fine (Section 4.0)	0.37 lbm
	Total	0.754 lbm

The total of 0.754 lbm represents 13% of the available 5.8 lbm of Freon 14. The Freon required in the computing networks could be collected and used in the reaction control system if desired.

The fluidic compensation consists of gain and a lead network. The gain is about the maximum value typically implemented with fluidics. The value also is about as high as can be tolerated by the loop before becoming unstable. The lead network provides the necessary compensation needed to stabilize the loop in the frequency region around the magnetometer second-order lead. The lag in the FPT is essential to the closed loop stability. If the FPT lag occurs at a higher frequency, a lag network should be added to the compensation to insure closed-loop stability.

The roll-position closed-loop transfer function was computed for three spatial orientations (i.e. values of $\cos\phi\sin\eta$). The results are:

For $\cos\phi\sin\eta = 1.0$ (e.g. $\phi = 0$ deg; $\eta = 90$ deg)

$$\frac{\delta\phi}{\delta\phi_c} \approx \frac{+22.5}{1 + \frac{2(.211)S}{5.43} + \frac{S^2}{(5.43)^2}} \quad \frac{deg}{psid} \tag{19}$$

For $\cos\phi\sin\eta = 0.5$ (e.g. $\phi = 45$ deg; $\eta = 45$ deg)

$$\frac{\delta\phi}{\delta\phi_c} \approx \frac{+45}{1 + \frac{2(.266)S}{2.91} + \frac{S^2}{(2.91)^2}} \quad \frac{deg}{psid} \tag{20}$$

For $\cos\phi\sin\eta = 0.0301$ (e.g. $\phi = 80$ deg; $\eta = 10$ deg)

$$\frac{\delta\phi}{\delta\phi_c} \approx \frac{+746}{(1 + \frac{2(.014)S}{.214} + \frac{S^2}{(.214)^2})(1 \frac{-2(.334)S}{469} + \frac{S^2}{(469)^2})} \quad \frac{deg}{psid} \tag{21}$$

It is important to note that the transfer functions in (19) and (20) are stable, but in (21) it is unstable. Since the magnetometer can be oriented to a desired position before a mission, it is possible to position it so the commanded angle corresponds to $\phi = 0$. This alone eliminates many of the possible unstable conditions. Also, missions usually are not attempted for $\eta = 10$ degrees which eliminates still more unstable conditions. Thus unstable situations corresponding to Eq. 21 are not expected to be encountered. A reasonable nominal orientation has a transfer function given by (19) or (20) both of which are stable. The responses of (19) and (20) to a step command of five degrees are shown in Figure 15. In both cases (Figure 15) the response to the step command is accompanied by ringing which is reasonably damped after five seconds. The ringing can be reduced by the addition of compensation to provide more phase margin in the vicinity of the open loop crossover frequency, but at the expense of increased implementation complexity.
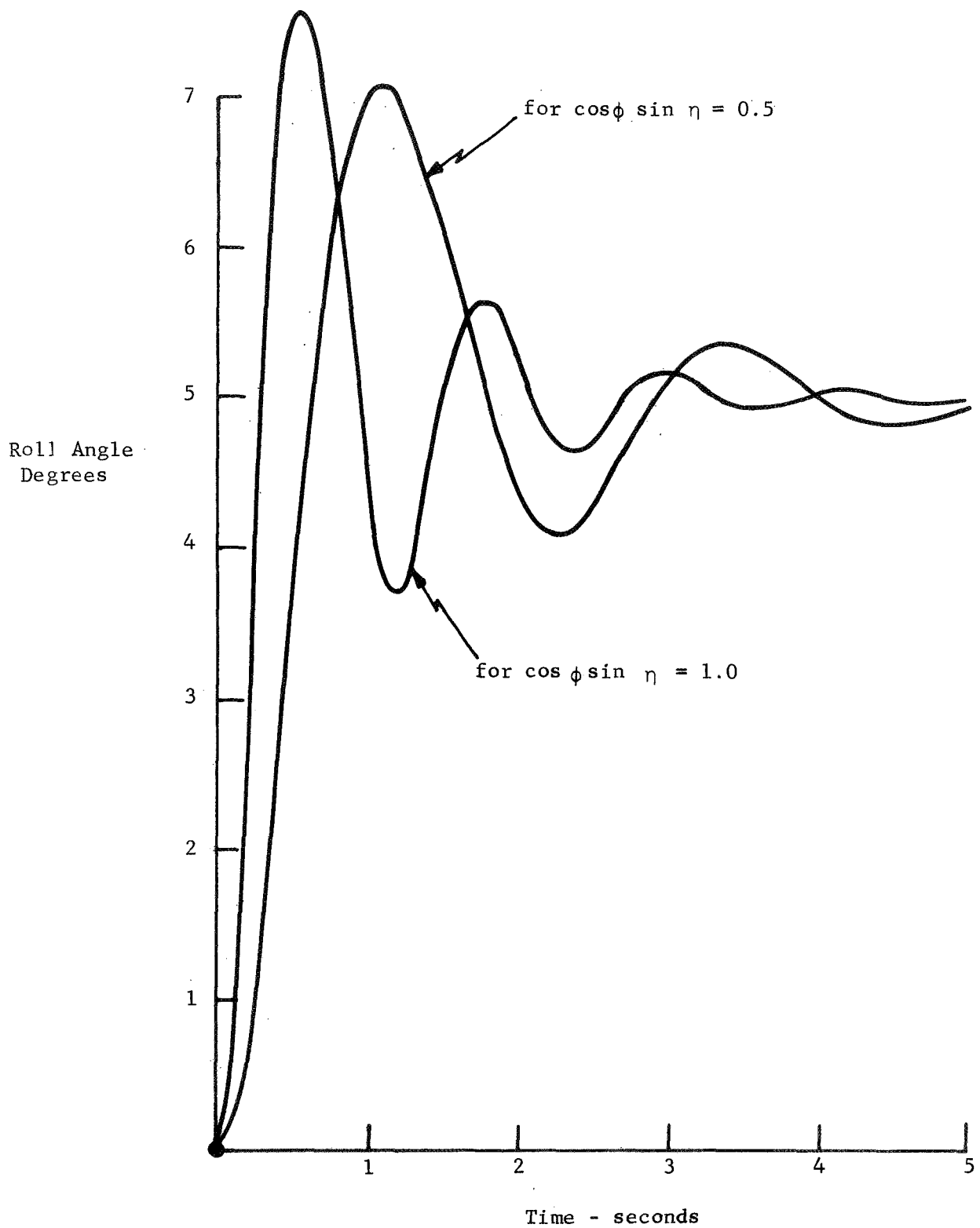
31

for $\cos\phi\,\sin\,\eta = 0.5$

for $\cos\phi\,\sin\,\eta = 1.0$

Roll Angle
Degrees

Time - seconds

Fig. 15 Roll Position Control Step Response.

APPENDIX I -NOMENCLATURE

A_c - control area on magnet

B - flux density in the magnet

d_m - diameter of magnet

H - earth's magnetic field

I_m - magnetometer bar moment of inertia

K_j - jet pipe gain

K_m - magnetic spring constant

K_r - flexpivot spring constant

K_1 - amplifier gain

L_c - distance from pivot to control ports around the magnet

L_m - magnet length

M - pole strength

M_m - mass of magnet

n - ratio of lag to lead break frequencies in lead network

P - pressure

Q - volume flow

R - gas constant

T - temperature

$\dot{W}$ - weight flow

ϕ - roll angle

ϕ_m - angular displacement of magnet to earth's magnetic field

ϕ_r - relative angular displacement of magnet to the frame

τ - torque on the magnet caused by interaction of the earth's magnet field with the poles of the magnet

ω - lead break frequency

The logic shown in Figure I would be employed to interface the fluidic roll control loops with the present SPARCS. For the purpose of explanation the electrical signal levels will be assumed to be one of two levels which are 0 and 1. Also, a 1 level is assumed to be capable of activating a solenoid and a 0 level of deactivating a solenoid. The following definition is assigned to the signals:

J, start mission signal	0 mission not started
	1 mission started
L, latching relay signal	0 despin complete
	1 despin incomplete
G, fine control signal	0 fine control not in progress
	1 fine control in progress
F, intermediate control signal	0 pitch and yaw errors > 10 degrees
	1 pitch and yaw errors < 10 degrees

The following truth table shows that the output of the AND gate in the despin channel activates the despin channel solenoid only if the mission has started and despin is incomplete.

J	L	J.L	
0	0	0)	
0	1	0)	deactivate
1	0	0)	
1	1	1	activate

As the truth table demonstrates, the despin channel solenoid is activated only when the mission has started (J = 1) and despin is incomplete (L = 1).

The following truth table shows that the NOR gate in the roll rate control channel will keep that channel activated during coarse and intermediate control.

L	G	L+G	$\overline{L+G}$	
0	0	0	1	activate
0	1	1	0)	
1	0	1	0)	deactivate
1	1	1	0)	

The truth table shows that the roll channel solenoid is activated only when despin is complete (L = O) and fine control is not in progress (G = O).

Roll position control is activated by the G switch taking the arbitrary value of 1 which it does at the beginning of inter- mediate control. The F switch signal remains at this value even during fine control, so no additional processing with the G switch signal is required. The logic provides overlapping of roll rate and roll-position control during intermediate control which is necessary to insure sufficient rate damping.

The AND gate which processes the F and $\bar{G}$ (negation of G) switch signals is used to select the acceleration level in the roll channel. It selects the high acceleration level by activating a solenoid in the FPT which causes the pressure level at the roll nozzles to increase about twentyfold over the pressure available with the solenoid deactivated. The following truth table provides the proof.

F	G	$\bar{G}$	$F \cdot \bar{G}$		
0	1	0	0	)	
0	0	1	0	)	deactivate
1	1	0	0	)	
1	0	1	1		activate

The truth table shows that the high thrust level is activated when the pitch and yaw errors are less than ten degrees (F = 1) and fine control is not in progress (G = 0) which is the desired result.

A lead network has a gain/frequency characteristic as shown in Figure 16.

Gain, db

slope = 20 db per decade

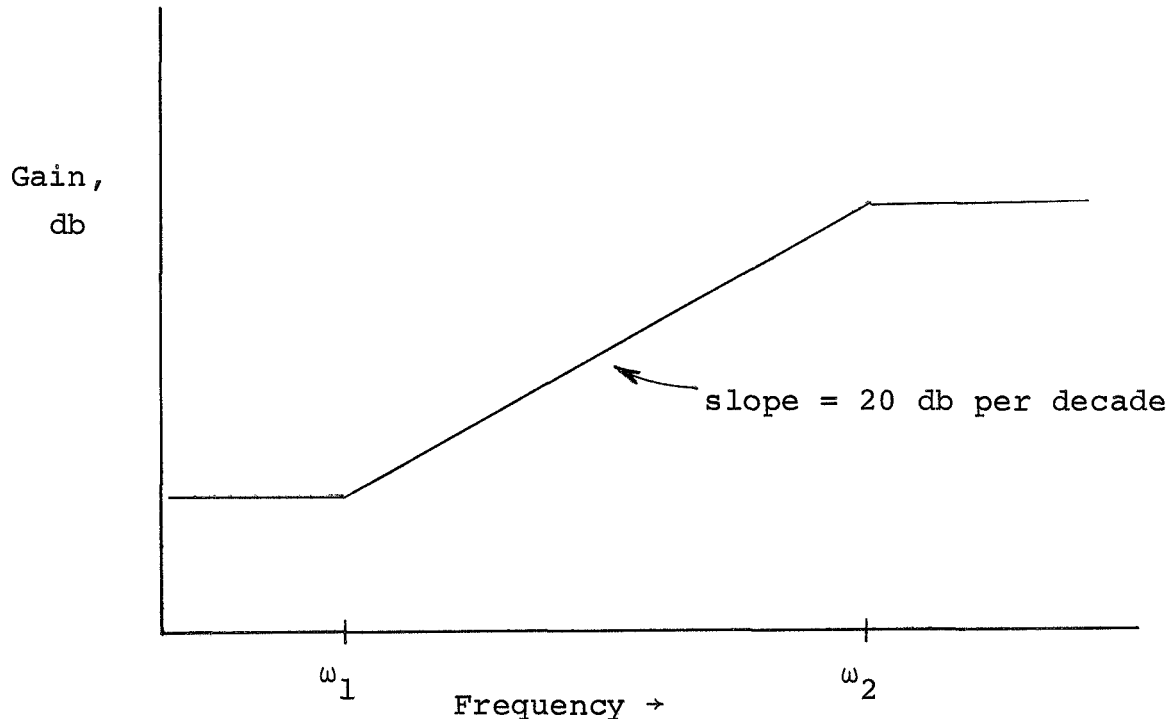ω_1

ω_2

Frequency →

Figure 16
Lead Network Frequency Response

As frequency increases the gain remains constant until the lead break frequency, ω_1, is reached. For increasing frequencies between ω_1 and ω_2 the gain increases at the rate of 20 db per decade. For frequencies greater than ω_2 the gain is again constant with increasing frequency. Because the lead occurs before the lag as frequency increases, a lag network is also called lead-lag compensation.

In the lead-lag compensation in Figure 8 the low frequency gain is constant and depends on the ratio of R_1 to R_2. R_1 and R_2 are the resistors inserted on either side of the control inputs. The gain will start to increase at the rate of 20 db per decade when the frequency is equal to $\omega_1 = (R_2+R_C)/(R_2R_CC)$. R_C is the control port resistance and C is the capacitance of the volume inserted on one side of the input. The gain increases bacause the resistance to ground at control port 2 starts to decrease at the rate of 20 db per

decade at the frequency ω_1. At control port 1 the resistance to ground ideally remains constant because there is no volume (i.e. capacitance) in the fluidic circuit. The gain will continue to increase until the maximum gain of the proportional amplifier is reached. The gain then remains constant for increasing frequency. The gain frequency characteristic of the compensation in Figure 6 is the same in form as that in Figure 14, so the compensation is a lead network (i.e. lead-lag compensation).